Research Article Vol. 8, No. 9 / September 2021 / Optica 1129

optica

Two-dimensional quantum walks of correlated photons

Zhi-Qiang Jiao,[1,2,†] Jun Gao,[1,2,†] Wen-Hao Zhou,[1,2] Xiao-Wei Wang,[1,2] Ruo-Jing Ren,[1,2] Xiao-Yun Xu,[1,2] Lu-Feng Qiao,[1,2] Yao Wang,[1,2] and Xian-Min Jin[1,2,*]

[1]Center for Integrated Quantum Information Technologies (IQIT), School of Physics and Astronomy and State Key Laboratory of Advanced Optical Communication Systems and Networks, Shanghai Jiao Tong University, Shanghai 200240, China
[2]CAS Center for Excellence and Synergetic Innovation Center in Quantum Information and Quantum Physics, University of Science and Technology of China, Hefei, Anhui 230026, China
*Corresponding author: xianmin.jin@sjtu.edu.cn

Received 22 March 2021; revised 19 July 2021; accepted 26 July 2021 (Doc. ID 425879); published 24 August 2021

Quantum walks in an elaborately designed graph are a powerful tool for simulating physical and topological phenomena, constructing novel quantum algorithms, and realizing universal quantum computing. Integrated photonics technology has emerged as a versatile platform for implementing a variety of quantum information tasks and as a promising candidate for performing large-scale quantum walks. Both extending physical dimensions and involving more particles will increase the complexity of the evolving systems. Pioneering studies have demonstrated a single particle walking on two-dimensional lattices and multiple walkers interfering on a one-dimensional structure. However, multiple particles evolving in a genuine two-dimensional space in a scalable fashion has remained a vacancy for nearly 10 years. We present a genuine two-dimensional quantum walk with correlated photons on a triangular photonic lattice, which is mapped to a 37 × 37 high-dimensional state space. The genuine two-dimensional quantum walk breaks through the physical restrictions of single-particle evolution, allowing for the encoding of information in large spaces and construction of high-dimensional graphs, which are beneficial for quantum information processing. Between the chip and the two-dimensional fanout interface, site-by-site addressing enables simultaneous detection of over 600 nonclassical interferences and observation of quantum correlations that violate a classical limit by 57 standard deviations. Our implementation provides a paradigm for multi-photon quantum walks in a two-dimensional configuration on a large scale, paving the way for practical quantum simulation and computation beyond the classical regime.

https://doi.org/10.1364/OPTICA.425879

1. INTRODUCTION

Random walks are widely utilized in physics, economics, and computer science. Due to their inherent quantum superposition, quantum walks (QWs) [1,2], the quantum extension of classical random walks, can even provide exponential speedups over classical random walks for specific problems [3]. This unique feature makes QWs an advanced approach to building quantum algorithms [3–7], simulating various transport processes such as energy transport in photosynthesis [8], light-harvesting molecules [9], perfect state transfer [10], coherent transport [11,12], as well as realizing universal quantum computation [13,14] and solving graph isomorphism problems [15]. Numerous QW experiments are implemented on diverse platforms, including nuclear magnetic resonance [16], trapped atoms and ions [17,18], superconducting systems [19], fibers [20,21], and especially integrated photonic systems [22–28] for the robust and coherent nature of photons.

An additional dimension may be advantageous for simulating hitherto unexplored physical phenomena in lower dimensions and for solving computationally difficult problems [29]. As shown in Fig. 1(a), efforts have been made to create physical and synthetic dimensions such as spatial mode, temporal loop, and momentum [29–38], which are physically limited in certain situations. For instance, it is difficult to expand spatial dimensions beyond three, and intrinsic light leakage makes it difficult for temporal modes to reach a sufficiently large scale. Despite the ballistic and transient natures demonstrated in these systems, the dynamics of a single particle can be simulated by classical light and exhibit no genuine quantum features [39]. Another possibility is to increase the number of walkers. Interferences or interactions between quantum walkers introduce nonclassical correlations that are not present in a single walker [23,25,26] and are thus impossible to simulate using classical particles [27,39]. In general, these quantum features exponentially extend Hilbert space with a linear increase in the number of quantum walkers [23,26], and may result in substantial speedups and quantum advantages over coherent light.

Simultaneously growing photon numbers and extending physical dimensions provide a scalable route to increasing graph complexity and connectivity, which are manifested as a graph's vertex number and the number of edges on a single vertex. However,

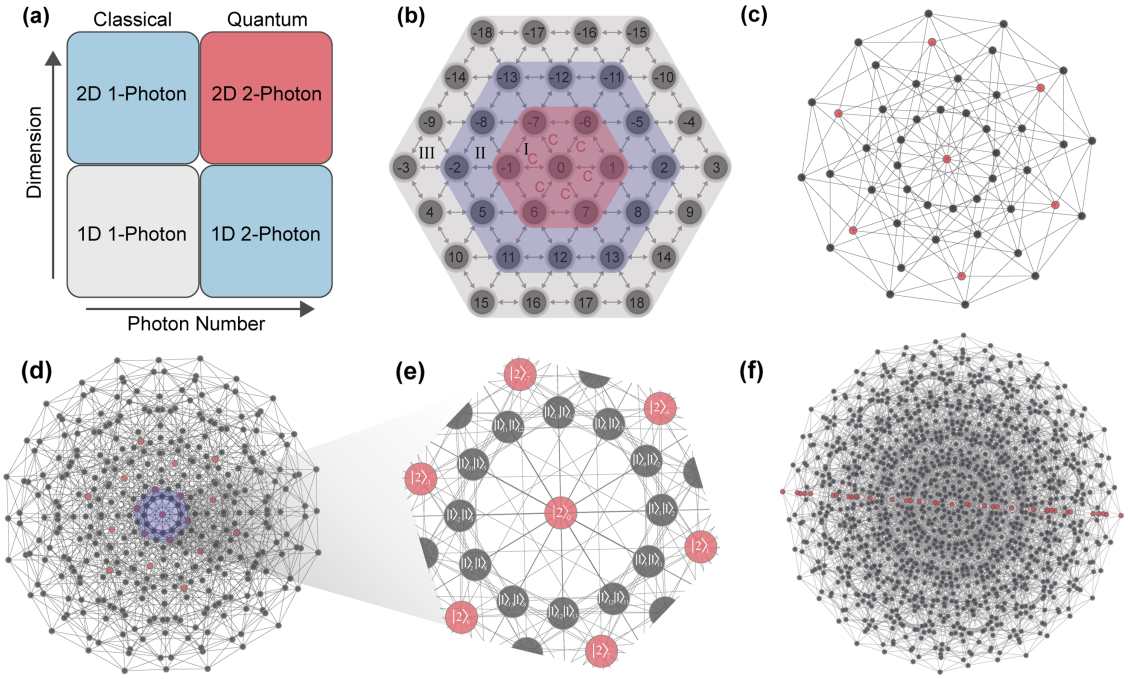

Fig. 1. Architecture for QWs and schematic of graph structures. (a) Both dimensions and photon numbers increase the complexity of photonic systems, embodied as a graph's vertex number and the number of edges on a single vertex. Single-particle QWs are under the description of classical wave theory. The graph dimensions are equal for two-photon 1D and single-photon 2D QWs, leaving the graph beyond 2D unexplored (red region). (b) Single-photon population graph structure. The state space of the single-photon population shares the same structure as the 2D lattice cross section. The coupling strength C is uniform for all adjacent nodes. The whole graph is divided into three layers to show the graph complexity. (c), (d) Sketch of high-dimensional graph structures spanned by a two-photon state injection, corresponding to seven sites (layer I) and 19 sites (layer II), respectively. Each node signifies a two-particle state with multiple edges showing flexible degrees of transitions. Every edge represents a possible transition between two-particle states. (e) Enlarged central part of (d). The site labels represent the photon basis states. Red ones are two-particle bunching states, while gray ones denote normal two-particle states. (f) Sketch of high-dimensional graph structures spanned by a two-photon state injection in the experiment (layer III), whose structure contains 1369 vertices and 6660 edges. The graph complexity grows exponentially with the photon number linear increase.

experimentally implementing such a scheme remains challenging owing to the lack of single-site addressing detection for tens of sites in 3D geometry. Efforts to implement 2D QWs with multiple photons have been made continuously. The previous attempt at arranging QWs in a quasi-physical 2D, "Swiss cross" configuration [26], has been achieved by a photonic lattice inscribed by the femtosecond laser direct-writing technique [40]. This design involves just one vertical column and does not fully exploit the 2D structure, restricting walkers' freedom of movement in all directions. In fact, the femtosecond laser direct-writing method is especially well suited for building 2D arrangements, and this technique was recently used to fabricate a large 2D lattice with up to 49×49 modes for implementing single-photon QWs [27].

Here, we experimentally demonstrate 2D QWs using correlated photons mapping to a graph with extraordinarily high dimensions and connectivity. The triangular lattice is sufficiently flexible to create a variety of 2D lattices based on its current structure, and its cross section is accurately prototyped to couple to a 2D fanout interface [see Supplement 1]. By injecting two indistinguishable photons into the 2D lattice, we observe distinct quantum interferences and quantum correlations that strongly violate the Cauchy–Schwarz inequality [41]. Our study provides a paradigm for constructing a general large-scale and high-dimensional optical platform suited for practical quantum simulation and quantum computing.

2. EXPERIMENT

The 2D photonic lattice is fabricated using the 3D femtosecond laser direct-writing technique [see Supplement 1 for fabrication details]. The coupling zone has a spacing of 15 μm between two adjacent sites. Following the interaction zone, the separation is adiabatically expanded to 35 μm while maintaining the same geometric structure as the 2D fanout architecture, as shown in the inset of Fig. 2(b). A distance of 35 μm between adjacent sites is sufficient to isolate photon hopping between them. Figure 1(b) shows the cross section of the 2D lattice, which represents the state space of single-photon populating $N = 37$ sites. Each site in the triangular lattice has six edges and homogenous coupling to its neighbors, providing a higher level of connectivity than square lattices. To demonstrate the graph's complexity, we divide it into three layers [Fig. 1(b)]. The graphs in Figs. 1(c) and 1(d) show the high-dimensional graphs spanned by a two-photon state injection, which correspond to seven sites (layer I) and 19 sites (layer II), respectively. The enlarged state space grows exponentially in scale as the number of injected particles increases. All sites in the graph represent the two-photon basis states, and the red ones are highlighted to emphasize the bunching states, as shown by the enlarged region in Fig. 1(e). The edges denote the hopping and transition between basis states. The connected graph generated in our experiment is shown in Fig. 1(f), which contains 1369 sites and 6660 edges [see Supplement 1 for calculation details].

The experimental setup is shown schematically in Figs. 2(a)–2(c), which depict quantum state preparations, on-chip unitary

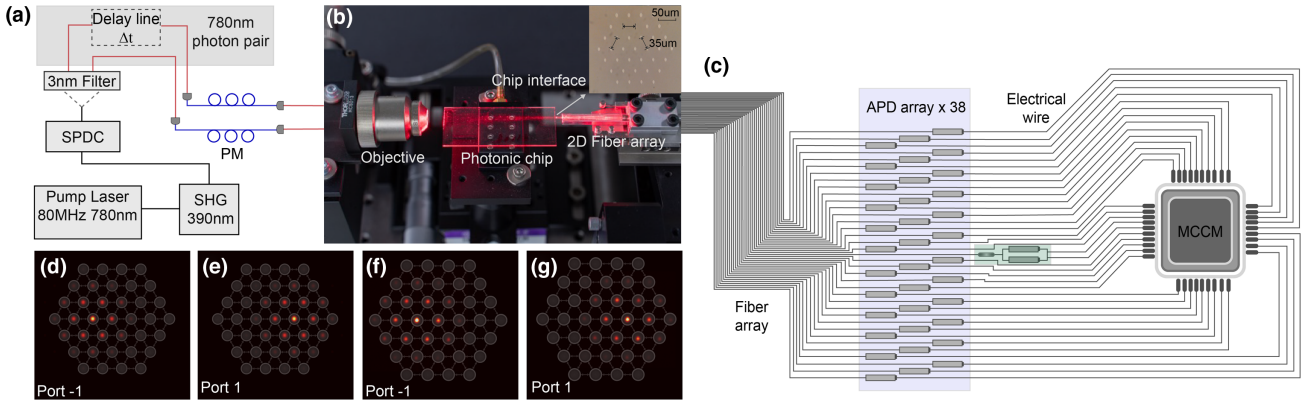

Fig. 2. Sketch of experimental implementation of 2D QWs of correlated photons. (a) Correlated photon pair generation. A 780 nm fs laser pumps a LiB_3O_5 (LBO) crystal to generate a 390 nm pulse by second-harmonic generation (SHG). Then the 390 nm UV pulse pumps a β-BaB_2O_4 (BBO) crystal via type-II phase-matching and generates photon pairs in a beam-like scheme. 3 nm bandpass filters filter the correlated photons. An external delay line in one of the setup arms adjusts the distinguishability of photons. (b) A 20× objective focuses the correlated photons into the photonic chip in free space. The inset shows the output 2D cross section of the chip. A 2D fanout is connected to the 3D photonic chip to achieve site-by-site couplings. (c) Diagram of the detection system. There are 38 APDs used in the experiment to detect single photon signals. The detecting system is connected to a homemade multi-channel coincidence module (MCCM), which captures all simultaneous clicks between any two APDs. The green zone shows the multiplexed detection of bunching events using a balanced fiber beam splitter. (d), (e) Simulated intensity distributions of photons injected into ports −1 and 1. (f), (g) Experimental intensity distributions of coherent light injected into ports −1 and 1 accumulated by a CCD.

operations, and large-scale coincident measurements, respectively. We produce upconverted 390 nm ultraviolet pulses using a 780 nm Ti:sapphire solid-state femtosecond laser pumping a LiB_3O_5 (LBO) crystal. Then, using the 390 nm pulses to pump a β-BaB_2O_4 (BBO) crystal fulfilling type-II phase-matching, correlated photons are generated in a beam-like scheme [42]. A 3 nm bandpass filter ensures spectrum indistinguishability by filtering the correlated photons. Temporal overlap is achieved via an external delay line with a motorized translation stage in one of the setup arms. Correlated photons are coupled into the photonic chip by a 20× objective in free space after appropriate polarization compensation. Through precise and accurate alignment, the coupling efficiency for both input ports exceeds 50%.

First, we inject coherent light into ports −1 and 1, and then use a charge-coupled device (CCD) to collect the output patterns of the chip. The probability distribution of photons can be extracted from the accumulated pattern, which has been extensively adopted in previous coherent light and single-photon experiments [27]. The experimental results are illustrated in Figs. 2(f) and 2(g) compared with theoretical simulations in Figs. 2(d) and 2(e). The similarity between the patterns is calculated as $S_i = \left(\sum_j \sqrt{p^{\exp}_{i,j} \cdot p^{\text{th}}_{i,j}}\right)^2 \Big/ \left(\sum_j p^{\exp}_{i,j} \sum_j p^{\text{th}}_{i,j}\right)$, with results of up to 99.6% ± 0.3% and 98.4% ± 0.3%, respectively. After characterization of the photonic chip, we then connect it to a 2D fanout fiber array [see Supplement 1] linked to an avalanche photodiode (APD) array, shown in Fig. 2(c). A homemade multi-channel coincidence module (MCCM) simultaneously records the coincidence counts of all two-channel combinations from the APD array for further processing.

3. RESULTS

As shown in Figs. 3(a) and 3(b), we reconstruct the probability distributions using single-photon injection instead of coherent light. The distributions are not significantly different from those in Fig. 2. In the case of two-photon injection, the probability

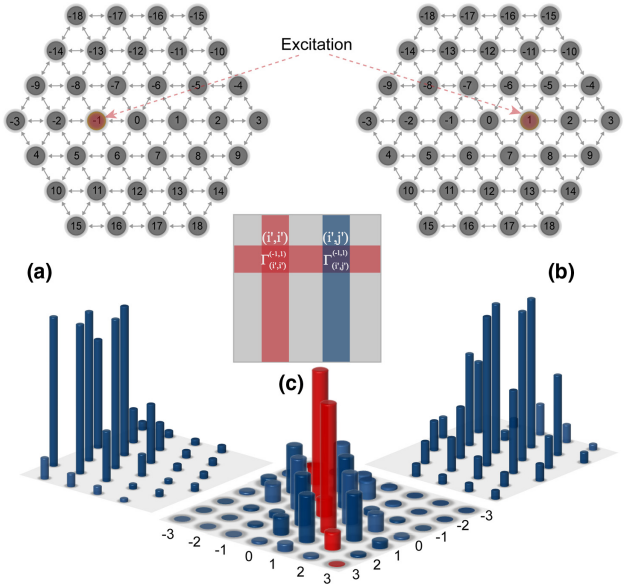

Fig. 3. Illustration of measuring quantum correlations. (a), (b) Single-photon probability distributions measured by the APD detection system for ports −1 and 1 injections, respectively. (c) Coincident counts are measured in the interference position to get the normalized coincident probability, which reveals two-photon quantum correlations $\Gamma^{(i,j)}_{i',j'}$. Parts of correlation are listed in coincident probability distributions. The red columns represent the probability of two photons bunching in the same waveguide, while the blue columns represent correlations between different waveguides. The graph's height is proportional to the intensity of quantum correlations.

distribution cannot reveal any quantum features since the result is equivalent to an incoherent sum of these two distributions. To describe the multi-particle interferences in the enlarged state space, the two-photon correlation function $\Gamma^{(i,j)}_{i',j'}$ is introduced [41,43]:

$$\Gamma^{(i,j)}_{i',j'} = \frac{1}{1+\delta_{i',j'}} \left| U_{i',i}(z) U_{j',j}(z) + U_{i',j}(z) U_{j',i}(z) \right|^2, \quad (1)$$

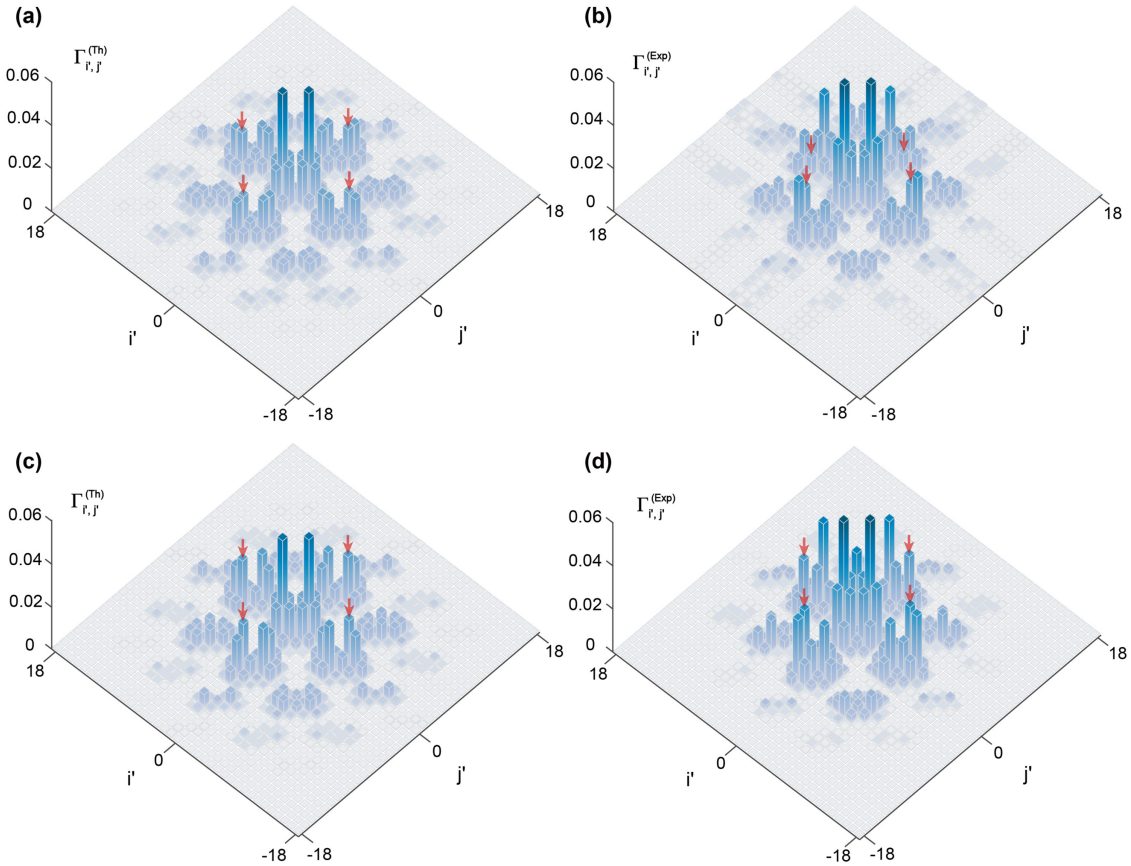

Fig. 4. Simulated and measured correlations. (a), (b) Theoretical and experimental correlations of distinguishable photons coupled to waveguide ports −1 and 1, respectively. The distinguishable photons are separated by temporal delay. The normalized probability distributions reveal the experimental classical correlations. (c), (d) Theoretical and experimental correlation matrix obtained from indistinguishable photons injected into ports −1 and 1. The photons are simultaneously injected into the triangular lattice, and quantum interferences spread over the lattice. The coincident counts are accumulated for 2000 s to get the normalized probability distributions, which reveal the quantum correlations. The quantum interferences make the probability distributions of quantum correlations [(c), (d)] different from classical ones [(a), (b)]. Some increasing parts in quantum correlations compared to classical correlations are labeled by red arrows.

where i, j are the input ports, while i', j' are the output ports. $U_{i',j}(z)$ represents the probability amplitude of detecting a photon in i' when injected in j [see Supplement 1]. Therefore, it is essential to perform coincidence measurements between each pair of sites and to enumerate all possible combinations, that is, to collect the simultaneous clicks from each pair of APDs at the interference point. Multiplexed detection with a balanced fiber splitter resolves the bunched photons at a single site [Fig. 2(c)], allowing us to get correlations at single sites.

We measure the complete quantum correlations when correlated photons are injected into ports −1 and 1. By varying the relative temporal delay, the degree of photon indistinguishability is adjusted. The MCCM simultaneously records all $\binom{37}{2} = 666$ Hong–Ou–Mandel (HOM) interference curves [44]. Simultaneous recording of all the coincidences is important, especially for database search algorithms such as Grover's algorithm [7]. The HOM interferences establish a connection between adjacent and non-adjacent photons populated on the 2D lattice shown in Figs. 3(a) and 3(b) at the interference position, for example, sites 2 and 11, which cannot be explored on a 1D array. Coincident counts between two different sites are acquired at the interference location. The bunched photons in single sites are resolved by a balanced beam splitter to retrieve the coincident counts. Data are collected for 2000 s to retrieve the complete quantum correlations. We get the coincident probability by normalizing the counts, which reveals the two-photon quantum correlations. Parts of the results are listed in Fig. 3(c) to illustrate the bunched coincidences in one site and correlations between two different sites. The classical correlations can be readily calculated by classical probability theory as $\Gamma^{(i,j)(c)}_{i',j'}(z) = p_{i',i}(z)p_{j',j}(z) + p_{i',j}(z)p_{j',i}(z)$, where p denotes the probability of detecting photons, i, j are input ports, and i', j' are output ports.

Figures 4(a) and 4(b) show the theoretical and experimental coincident probabilities of distinguishable photons, respectively. The distinguishable photon pair is separated with a time delay using a high-precision stage. Quantum correlations are shown theoretically and experimentally in Figs. 4(c) and 4(d) when photons are simultaneously injected into the triangular lattice. Due to the quantum interference, the coincident probability distributions of quantum correlations [Figs. 4(c) and 4(d)] differ from classical ones [(a), (b)]. Some of the quantum correlations will decrease, while others will increase. The red arrows indicate a portion of the growing quantum correlations in comparison to classical correlations. Meanwhile, the quantum interference

guarantees that an expanded high-dimensional graph emerges rather than a mere incoherent sum of distinct photon distributions. We calculate the similarity between the two matrices defined by $S = \left(\sum_{i,j} \sqrt{\Gamma^{\mathrm{exp}}_{i,j} \cdot \Gamma^{\mathrm{th}}_{i,j}}\right)^2 \Big/ \left(\sum_{i,j} \Gamma^{\mathrm{exp}}_{i,j} \sum_{i,j} \Gamma^{\mathrm{th}}_{i,j}\right)$ to characterize the discrepancy between experiment and theory. Finally, the experiment results reveal a similarity of $91.8\% \pm 0.1\%$ with regard to the simulation. The deviation comes from the imperfection of photon indistinguishability and the differential coupling efficiency in the 2D fanout. The standard adjacent pitch deviation of the 2D fanout is about 1 μm, resulting in a small coupling loss for certain channels.

As shown in Fig. 1(a), we get a 2D graph with limited connectivity from a 1D lattice with correlated photons. This graph structure is identical to that of a 2D lattice with single-photon or classical light injections. Moreover, in a scalable fashion, the triangular lattice has more edges than square lattices for one vertex. When combined with indistinguishable photons, we can exponentially enlarge the state space to get a high-complex graph suitable for solving specific quantum tasks [15]. Additionally, it can generate a variety of 2D lattices, including a hexagonal lattice and Kagome lattice, to meet diverse applications [see Supplement 1]. Technically, the 1D waveguide array can be coupled to a commercial V-grooved fiber array with designed spacing. However, for 2D QWs, the situation becomes extremely difficult. Previous studies have transformed the 2D structure into a 1D alignment to match the commercial fiber array [26], but this approach inevitably introduces differential losses for different channels and may result in unpredictable couplings during the transformation. We overcome this bottleneck by directly mapping the 2D cross section to a 2D fanout interface and connecting the output fibers to the APD array shown in Fig. 2(c) [see Supplement 1], thus ushering the QWs into a new era, a genuine quantum domain, in a scalable 2D fashion.

To obtain a complete description of photon pair interference in a 2D lattice, the bunching effect must be verified using a balanced fiber beam splitter. Due to the high-count rates in site 0, we collect 200 s coincident counts in each data point from the balanced beam splitter by smoothly shifting the stage in a 40 μm interval. As shown in Fig. 5(a), the peak value is nearly twice that of distinguishable values, with visibility of up to $92\% \pm 3.5\%$ for site 0. The Cauchy–Schwarz inequality is measured to quantify the quantum bunching effect observed in the 2D lattice. According to the inequality, correlations in the diagonal $\Gamma_{i,i}$ are related to correlations in the off-diagonal $\Gamma_{i,j}$ and $i \neq j$ [41]:

$$V_{i,j} = \frac{2}{3}\sqrt{\Gamma^{c}_{i,i}\Gamma^{c}_{j,j}} - \Gamma^{c}_{i,j} < 0, \tag{2}$$

with Γ^c here referring to intensity correlations between classical light beams. The violation of the Cauchy–Schwarz inequality quantifies the nonclassical nature of the measured quantum correlations. We substitute Γ^c with quantum correlations $\Gamma^{(1,-1)(q)}_{i',j'}$ obtained from experiment to test Eq. (2) beyond the classical limit. Their number of standard deviations is estimated by assuming the two photons follow Possonian statistics. Violations of classical limits are spread over the 2D lattice, and the maximum standard deviation of violations is up to 57, as depicted in Fig. 5(b). These results reveal that a 2D lattice with indistinguishable photons produces genuine 2D QWs and enables new possible transitions populated over the high-dimensional graph that cannot be realized in a 1D lattice.

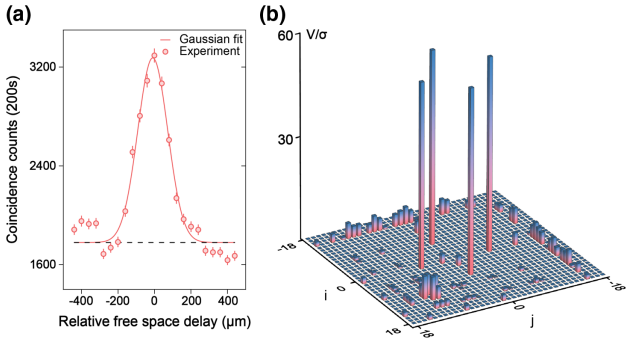

Fig. 5. Nonclassical certification of two-photon QWs. (a) Photon bunching curve retrieved from site 0. By continuously shifting the relative free-space delay between these two photons, a distinct quantum interference peak is observed for site 0. This typical interference curve shows the visibility of $92\% \pm 3.5\%$. (b) Violations of the Cauchy–Schwarz inequality. These violations are certified by the standard deviations σ, assuming individual counts follow Poissonian statistics. The histograms in red represent violations. The maximum standard deviation of violations is up to 57. Only indistinguishable photons exhibit bosonic bunching features that enable the appearance of violations as expected.

4. CONCLUSION AND DISCUSSION

To conclude, we have experimentally demonstrated genuine spatial 2D QWs of correlated photons and verified two-particle quantum bunching effects through simultaneous measurements. We observe a strong violation of the Cauchy–Schwarz inequality Eq. (2) from quantum correlations that cannot be simulated in classical systems. Our experimental scheme overcomes the 2D single-site addressing detection limit in quantum regimes, allowing for the manipulation of multiple photons in a largely sophisticated 2D lattice. Through site-by-site addressing of 2D interface coupling and large-scale coincident measurements, the generated high-dimensional graph may be applied to a number of practical applications. Multi-photon walkers combined with this genuinely scalable 2D arrangement exponentially enlarge the state space, making it particularly suited for constructing quantum search algorithms, such as Grover algorithms [7], and a possible way to exhibit quantum advantages [45,46] over classical supercomputers.

Beyond the standard model, many experimentally unexplored areas in higher dimensions deserve further investigations, including the effect of multi-photon localization, as well as the dynamics and transport properties of multiple photons in 2D complex quantum systems. Along with the flexibility of the input photon number states, other quantum states, such as entanglement states or N00N states that interact in a topological system, remain to be investigated under 2D boundary conditions. Additionally, our scalable experimental architecture with integrated sources [47,48] may pave the way for the development of large-scale integrated quantum simulation and analog quantum computing, even for the near-term noisy intermediate-scale quantum (NISQ) technologies [49].

Funding. Shanghai Municipal Education Commission (SMEC) (2017-01-07-00-02-E00049); Science and Technology Commission of Shanghai Municipality (STCSM) (17JC1400403); National Natural Science Foundation of China (NSFC) (11690033, 11761141014, 61734005); National Key Research and Development Program of China (2017YFA0303700, 2019YFA0308700).

Acknowledgment. The authors thank Roberto Osellame and Jian-Wei Pan for helpful discussions. X.-M. J. acknowledges additional support from a Shanghai

talent program and from Zhiyuan Innovative Research Center of Shanghai Jiao Tong University.

Disclosures. The authors declare no conflicts of interest.

Data availability. Data underlying the results presented in this paper are not publicly available at this time but may be obtained from the authors upon reasonable request.

Supplemental document. See Supplement 1 for supporting content.

†These authors contributed equally to this paper.

REFERENCES

1. Y. Aharonov, L. Davidovich, and N. Zagury, "Quantum random walks," Phys. Rev. A **48**, 1687–1690 (1993).
2. E. Farhi and S. Gutmann, "Quantum computation and decision trees," Phys. Rev. A **58**, 915-928 (1998).
3. A. M. Childs, R. Cleve, E. Deotto, E. Farhi, S. Gutmann, and D. A. Spielman, "Exponential algorithmic speedup by a quantum walk," in *35th ACM Symposium on Theory of Computing (STOC)* (2003), pp. 59-68.
4. A. M. Childs and J. Goldstone, "Spatial search by quantum walk," Phys. Rev. A **70**, 022314 (2004).
5. A. Ambainis, "Quantum walks and their algorithmic applications," Int. J. Quantum Inf. **1**, 507-518 (2003).
6. N. Shenvi, J. Kempe, and K. B. Whaley, "Quantum random-walk search algorithm," Phys. Rev. A **67**, 052307 (2003).
7. C. D. Franco, M. M. Gettrick, and T. Busch, "Mimicking the probability distribution of a two-dimensional Grover walk with a single-qubit coin," Phys. Rev. Lett. **106**, 080502 (2011).
8. M. Mohseni, P. Rebentrost, S. Lloyd, and A. A. Guzik, "Environment-assisted quantum walks in photosynthetic energy transfer," J. Chem. Phys. **129**, 174106 (2008).
9. M. B. Plenioand and S. F. Huelga, "Dephasing-assisted transport: quantum networks and biomolecules," New J. Phys. **10**, 113019 (2008).
10. V. M. Kendon and C. Tamon, "Perfect state transfer in quantum walks on graphs," J. Comput. Theor. Nanos. **8**, 422-433 (2011).
11. O. Mülken and A. Blumen, "Continuous-time quantum walks: models for coherent transport on complex networks," Phys. Rep. **502**, 37-87 (2011).
12. D. N. Biggerstaff, R. Heilmann, A. A. Zecevik, M. Gräfe, M. A. Broome, A. Fedrizzi, S. Nolte, A. Szameit, A. G. White, and I. Kassal, "Enhancing coherent transport in a photonic network using controllable decoherence," Nat. Commun. **7**, 11282 (2016).
13. A. M. Childs, "Universal computation by quantum walk," Phys. Rev. Lett. **102**, 180501 (2009).
14. A. M. Childs, D. Gosset, and Z. Webb, "Universal computation by multiparticle quantum walk," Science **339**, 791-794 (2013).
15. J. K. Gamble, M. Friesen, D. Zhou, R. Joynt, and S. N. Coppersmith, "Two-particle quantum walks applied to the graph isomorphism problem," Phys. Rev. A **81**, 052313 (2010).
16. J.-F. Du, H. Li, X.-D. Xu, M.-J. Shi, J.-H. Wu, X.-Y. Zhou, and R.-D. Han, "Experimental implementation of the quantum random-walk algorithm," Phys. Rev. A **67**, 042316 (2003).
17. M. Karski, L. Förster, J.-M. Choi, A. Steffen, W. Alt, D. Meschede, and A. Widera, "Quantum walk in position space with single optically trapped atoms," Science **325**, 174-177 (2009).
18. H. Schmitz, R. Matjeschk, C. Schneider, J. Glueckert, M. Enderlein, T. Huber, and T. Schaetz, "Quantum walk of a trapped ion in phase space,", Phys. Rev. Lett. **103**, 090504 (2009).
19. Z.-G. Yan, Y.-R. Zhang, M. Gong, Y.-L. Wu, Y.-R. Zheng, S.-W. Li, C. Wang, F.-T. Liang, J. Lin, Y. Xu, C. Guo, L.-H. Sun, C.-Z. Peng, K.-Y. Xia, H. Deng, H. Rong, J.-Q. You, F. Nori, H. Fan, X.-B. Zhu, and J.-W. Pan, "Strongly correlated quantum walks with a 12-qubit superconducting processor," Science **364**, 753-756 (2019).
20. A. Schreiber, K. N. Cassemiro, V. Potoček, A. Gábris, P. J. Mosley, E. Andersson, I. Jex, and C. Silberhorn, "Photons walking the line: a quantum walk with adjustable coin operations," Phys. Rev. Lett. **104**, 050502 (2010).
21. H. Defienne, M. Barbieri, I. A. Walmsley, B. J. Smith, and S. Gigan, "Two-photon quantum walk in a multimode fiber," Sci. Adv. **2**, e1501054 (2016).
22. H. B. Perets, Y. Lahini, F. Pozzi, M. Sorel, R. Morandotti, and Y. Silberberg, "Realization of quantum walks with negligible decoherence in waveguide lattices," Phys. Rev. Lett. **100**, 013906 (2008).
23. A. Peruzzo, M. Lobino, J. C. F. Matthews, N. Matsuda, A. Politi, K. Poulios, X.-Q. Zhou, Y. Lahini, N. Ismail, K. Wörhoff, Y. Bromberg, Y. Silberberg, M. G. Thompson, and J. L. OBrien, "Quantum walks of correlated photons," Science **329**, 1500-1503 (2010).
24. J. O. Owens, M. A. Broome, D. N. Biggerstaff, M. E. Goggin, A. Fedrizzi, T. Linjordet, M. Ams, G. D. Marshall, J. Twamley, M. J. Withford, and A. G. White, "Two-photon quantum walks in an elliptical direct-write waveguide array," New J. Phys. **13**, 075003 (2011).
25. L. Sansoni, F. Sciarrino, G. Vallone, P. Mataloni, A. Crespi, R. Ramponi, and R. Osellame, "Two-particle Bosonic-Fermionic quantum walk via integrated photonics," Phys. Rev. Lett. **108**, 010502 (2012).
26. K. Poulios, R. Keil, D. Fry, J. D. A. Meineche, J. C. F. Matthews, A. Politi, M. Lobino, M. Gräfe, M. Heinrich, S. Nolte, A. Szameit, and J. L. O'Brien, "Quantum walks of correlated photon pairs in two-dimensional waveguide arrays," Phys. Rev. Lett. **112**, 143604 (2014).
27. H. Tang, X.-F. Lin, Z. Feng, J.-Y. Chen, J. Gao, K. Sun, C.-Y. Wang, P.-C. Lai, X.-Y. Xu, Y. Wang, L.-F. Qiao, A.-L. Yang, and X.-M. Jin, "Experimental two-dimensional quantum walk on a photonic chip," Sci. Adv. **4**, eaat3174 (2018).
28. H. Tang, C. Di Franco, Z.-Y. Shi, T.-S. He, Z. Feng, J. Gao, K. Sun, Z.-M. Li, Z.-Q. Jiao, T.-Y. Wang, M. S. Kim, and X.-M. Jin, "Experimental quantum fast hitting on hexagonal graphs," Nat. Photonics **12**, 754-758 (2018).
29. A. Schreiber, A. Gábris, P. P. Rohde, K. Laiho, M. Štefaňák, V. Potoček, C. Hamilton, I. Jex, and C. Silberhorn, "A 2D quantum walk simulation of two-particle dynamics," Science **336**, 55-58 (2012).
30. M. Gräfe, A. S. Solntsev, R. Keil, A. A. Sukhorukov, M. Heinrich, A. Tünnermann, S. Nolte, A. Szameit, and Y. S. Kivshar, "Biphoton generation in quadratic waveguide arrays: a classical optical simulation," Sci. Rep. **2**, 562 (2012).
31. S. Longhi, "Photonic Bloch oscillations of correlated particles," Opt. Lett. **36**, 3248-3250 (2011).
32. M. Lebugle, M. Gräfe, R. Heilmann, A. Perez-Leija, S. Nolte, and A. Szameit, "Experimental observation of N00N states Bloch oscillations," Nat. Commun. **6**, 8273 (2015).
33. C. Chen, X. Ding, J. Qin, Y. He, Y.-H. Luo, M.-C. Chen, C. Liu, X.-L. Wang, W.-J. Zhang, H. Li, L.-X. You, Z. Wang, D.-W. Wang, B. C. Sanders, C.-Y. Lu, and J.-W. Pan, "Observation of topologically protected edge states in a photonic two-dimensional quantum walk," Phys. Rev. Lett. **121**, 100502 (2018).
34. A. D'Errico, F. Cardano, M. Maffei, A. Dauphin, R. Barboza, C. Esposito, B. Piccirillo, M. Lewenstein, P. Massignan, and L. Marrucci, "Two-dimensional topological quantum walks in the momentum space of structured light," Optica **7**, 108-114 (2020).
35. O. Zilberberg, S. Huang, J. Guglielmon, M. Wang, K. P. Chen, Y. E. Kraus, and M. C. Rechtsman, "Photonic topological boundary pumping as a probe of 4D quantum Hall physics," Nature **553**, 59-62 (2018).
36. E. Lustig, S. Weimann, Y. Plotnik, Y. Lumer, M. A. Bandres, A. Szameit, and M. Segev, "Photonic topological insulator in synthetic dimensions," Nature **567**, 356-360 (2019).
37. L. J. Maczewsky, K. Wang, A. A. Dovgiy, A. E. Miroshnichenko, A. Moroz, M. Ehrhardt, M. Heinrich, D. N. Christodoulides, A. Szameit, and A. A. Sukhorukov, "Synthesizing multi-dimensional excitation dynamics and localization transition in one-dimensional lattices," Nat. Photonics **14**, 76-81 (2019).
38. H. Chalabi, S. Barik, S. Mittal, T. E. Murphy, M. Hafezi, and E. Waks, "Synthetic gauge field for two-dimensional time-multiplexed quantum random walks," Phys. Rev. Lett. **123**, 150503 (2019).
39. P. L. Knight, E. Roldán, and J. E. Sipe, "Quantum walk on the line as an interference phenomenon," Phys. Rev. A **68**, 020301 (2003).
40. A. Szameit and S. Nolte, "Discrete optics in femtosecond-laser-written photonic structures," J. Phys. B **43**, 163001 (2010).
41. Y. Bromberg, Y. Lahini, R. Morandotti, and Y. Silberberg, "Quantum and classical correlations in waveguide lattices," Phys. Rev. Lett. **102**, 253904 (2009).
42. Y. H. Kim, "Quantum interference with beamlike type-II spontaneous parametric down-conversion," Phys. Rev. A **68**, 013804 (2003).
43. K. Mattle, M. Michler, H. Weinfurter, A. Zeilinger, and M. Zukowski, "Non-classical statistics at multiport beam splitters," Appl. Phys. B **60**, S111-S117 (1995).

44. C.-K. Hong, Z.-Y. Ou, and L. Mandel, "Measurement of subpicosecond time intervals between two photons by interference," Phys. Rev. Lett. **59**, 2044–2046 (1987).
45. F. Arute, K. Arya, and R. Babbush, et al., "Quantum supremacy using a programmable superconducting processor," Nature **574**, 505-510 (2019).
46. H.-S. Zhong, H. Wang, and Y.-H. Deng, et al., "Quantum computational advantage using photons," Science **6523** 1460-1463 (2020).
47. L.-T. Feng, G.-C. Guo, and X.-F. Ren, "Progress on integrated quantum photonic sources with silicon," Adv. Quantum Technol. **3**, 1900058 (2020).
48. R.-J. Ren, J. Gao, W.-H. Zhou, Z.-Q. Jiao, L.-F. Qiao, X.-W. Wang, and X.-M. Jin, "128 Identical quantum sources integrated on a single silica chip," arXiv:2005.12918 (2020).
49. J. Preskill, "Quantum computing in the NISQ era and beyond," Quantum **2**, 79 (2018).